Research Journal of Applied Sciences, Engineering and Technology 6(11): 1984-1992, 2013
ISSN: 2040-7459; e-ISSN: 2040-7467

Submitted: November 24, 2012 Accepted: January 01, 2013 Published: July 25, 2013

Creep Crack Growth Modeling of Low Alloy Steel using Artificial Neural Network

F. Djavanroodi
Department of Mechanical Engineering, College of Engineering, Qassim University, KSA

Abstract: Prediction of crack growth under creep condition is prime requirement in order to avoid costly and time-consuming creep crack growth tests. To predict, in a reliable way, the growth of a major crack in a structural components operating at high temperatures, requires a fracture mechanics based approach. In this Study a novel technique, which uses Finite Element Method (FEM) together with Artificial Neural Networks (ANN) has been developed to predict the fracture mechanics parameter (C*) in a 1%Cr1%MoV low alloy rotor steel under wide range of loading and temperatures. After confirming the validity of the FEM model with experimental data, a collection of numerical and experimental data has been used for training the various neural networks models. Three networks have been used to simulate the process, the perceptron multilayer network with tangent transfer function that uses 9 neurons in the hidden layer, gives the best results. Finally, for validation three case studies at 538°C, 550°C and 594°C temperatures are employed. The proposed model has proved that a combinations of ANN and FEM simulation performs well in estimation of C* and it is a powerful designing tool for creep crack growth characterization.

Keywords: ANN, creep, failure analysis, FEM, fracture mechanics parameter (C*)

INTRODUCTION

Creep crack growth parameter (C^*): Under constant load at high temperatures metals exhibit creep deformation. Generally, there are three stages for creep deformation, namely primary, secondary and tertiary creep stages as shown in Fig. 1. For many materials, under steady state conditions (secondary creep rate) the stress and creep strain rate, may follow Norton's creep law; $\dot{\varepsilon}_s^c = A_s\sigma^{n_s}$, where A and n are material constants (which may depend on temperature). A component, even prior to service, may contain a number of pre-existing defects in the form of cracks. At elevated temperatures a body containing a defect may fail by creep rupture, fast fracture, creep crack growth or a combination of these processes. When subjected to stress at elevated temperatures creep crack growth may take place by the linking of voids and micro cracks that are generated on grain boundaries ahead of the crack tip. Failure by creep crack growth is generally found to be inter-granular processes (Webster and Ainsworth, 1994).

Elastic-plastic fracture mechanics theory has been modified to correlate the high temperature crack growth data. The C* integral has been used to characterize the creep crack growth (Webster and Ainsworth, 1994; Rice, 1968; Yatomi *et al*., 2006). Under steady-state conditions, the crack tip stress and strain rate fields are characterized by the creep crack growth parameter C^*. For a power law creeping material, C* is given as a path independent line integral:

$$C^* = \int_\Gamma \left[W_s^* dy - T_i(\delta\dot{u}_i/\delta_x)ds\right] \quad (1)$$

where,

Γ = The line integration path
ds = The length along the path Γ
W^* = Strain energy density change rate
T = The temperature

$$W_s^* = \int_o^{\dot{\varepsilon}_{ij}^c} \sigma_{ij} d\dot{\varepsilon}_{ij}^c \quad (2)$$

where ($\dot{u}_i = du_i/dt$) is displacement rate. The stress and strain rate around a crack tip can be expressed by C^* integral.

$$\sigma_{ij} = \sigma_o\left(\frac{C^*}{I_n\sigma_o\dot{\varepsilon}_o r}\right)^{1/(n+1)}\tilde{\sigma}_{ij}(\theta,n) \quad (3)$$

$$\dot{\varepsilon}_{ij} = \dot{\varepsilon}_o\left(\frac{C^*}{I_n\sigma_o\dot{\varepsilon}_o r}\right)^{n/(n+1)}\tilde{\varepsilon}_{ij}(\theta,n) \quad (4)$$

where, r and θ measure distance and polar angle relative to the crack tip, I_n is a parameter which depends only on the creep exponent, n; $\tilde{\sigma}_{ij}$ and $\tilde{\varepsilon}_{ij}$ are dimensionless functions. The parameter C^* may also be interpreted as an energy release rate (Webster and Ainsworth, 1994; Rice, 1968; Yatomi *et al*., 2006).

$$C^* = \frac{1}{B}\frac{dU^*}{da} \quad (5)$$

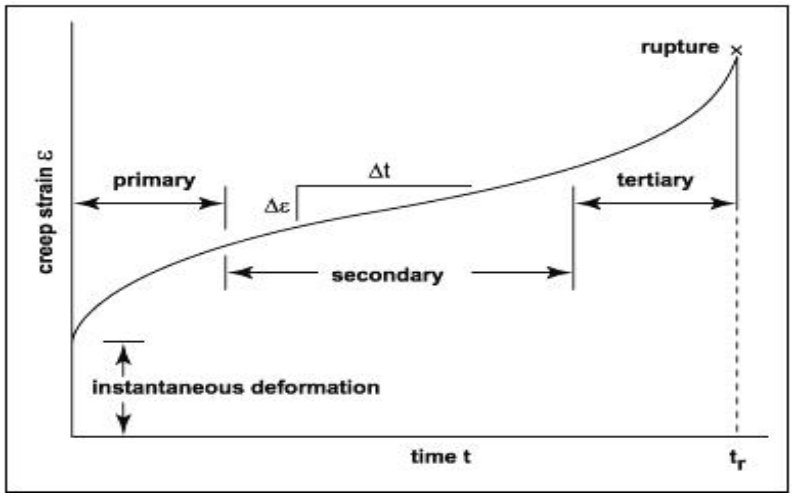

Fig. 1: Schematic of creep strain versus time (Djavanroodi and Nikbin, 2006)

where,
a = The crack length
B = The thickness
U^* = The potential energy rate

This implies that C^* can be calculated from data of force versus load–line displacement rate. In laboratory tests, C^*= Determined from the creep load-line displacement rate, according to ASTM E1457-01:

$$C^* = F\frac{P\dot{\Delta}^C}{B_n b} \quad (6)$$

where,
P = The applied load
b = The remaining ligament ahead of the crack
B_n = The net thickness (B_n = B for a specimen without side grooves).

The factor, F, depends on geometry and creep exponent, n: For a CT specimen F is given by ASTM E1457-01 (2002) and Djavanroodi and Nikbin (2006):

$$F = \frac{2+0.552\left(1-\frac{a}{w}\right)}{1-\frac{a}{w}} \quad (7)$$

where,
a = Crack length and W the specimen width.

In recent years, technical requirements for designing against fracture failure at high temperature are more demanding. It is difficult to determine the optimal design and working parameters by traditional approach, such as the use of experimental data or FEM approach. Analytical analysis of C^* parameter is a complex process, mainly because of the limited experimental data and analytical functions required for calculations, which usually involves the solution of complex differential equations. In order to simplify this complex process, a methodology has been developed to predict C*. The capability of the developed model is also investigated.

Artificial Neural Networks (ANN): In the past twenty years, Neural Networks Technique (NN) has been widely applied into many areas of engineering, such as control system, pattern recognition, system identification, decision making and so on. Neural networks has shown to have powerful learning capability and through a simple training procedure, the neural network can automatically develop the highly complex and nonlinear relationships between input variables and output features of training data (Freeman and Skapura, 1992). Optimal performance of neural network depends on, adequate quantity of experimental data, optimized architectures and efficient and convergent learning algorithm for the specific problem under investigation. Under these conditions, it then becomes possible to generate satisfactory results when presented with any new input data it has never experienced before. Also it has been recommended that physical models should be used wherever possible to supplement neural network models (Sha and Edwards, 2007). In the recent years, there has been increasing interest in neural network modeling in different fields of materials modeling (Mohanty *et al*., 2010; Toktas and Ozdemir, 2011; Mandal *et al*., 2009; Hou *et al*., 2010), most of them used Multi-Layer Perceptron (MLP) networks to predict desire outputs. However, Radial Basis Function (RBF) has been described as potential alternative approach to replace MLP networks in many research areas because this network offers some advantages such as robustness to noisy data, compared with MLP (Fathi and Aghakouchak, 2007). They investigated crack in welded T-butt joints using four MLP networks under membrane and bending.

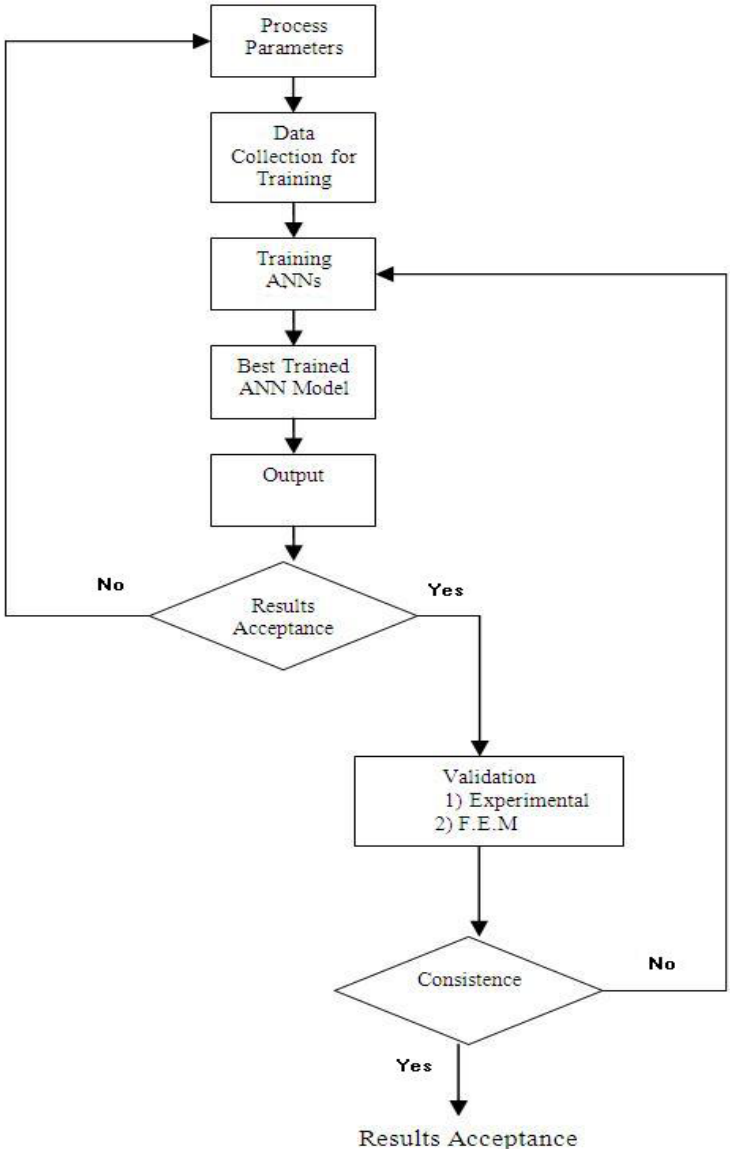

Fig. 2: Integrated FEM and ANN framewor

They concluded that the solution procedure and subsequently prediction by means of ANN are highly dependent on the quality and quantity of training database. Tapkin *et al*. (2009) successfully used Artificial Neural Networks (ANN) for the prediction of accumulated strain values obtained at the end of creep tests for Polypropylene (PP). Di Lorenzo *et al*. (2006) applied a combination of FEM and ANN to predict ductile fracture in cold forming operation. Talebi Anaraki *et al*. (2008) studied the relation between flow stress to strain, strain rate and the temperature for AZ61 Mg alloy and applied artificial neural network for modeling the rheological behavior of the this alloy. They showed a good agreement between predicted results by ANN and the experimental data. Hwang *et al*. (2010) used three independent neural network models for predicting the mechanical properties of rolled steel. This artificial intelligent analysis process has improved the quality of steel bar manufactured and also reduced the running cost of steel company due to the failure of bar's manufacture.

The objective of this study is to establish fracture mechanics models based upon the various neural networks for predicting the C^* parameter. Firstly, a series of experiments was performed by varying the load and initial crack length. An axi-symmetric elastic-creep, nonlinear analysis was performed by Finite element analysis for modeling the compact tension specimen, in a wide range of temperatures, forces and dimensions. After confirming the validity of the FEM model with experimental data, a collection of numerical and experimental data at 538, 550 and 594°C, respectively temperatures are employed to train the various neural networks models. These data was divided into three parts: training, test and validation

Table 1: Composition of the 1CrMoV rotor steel (% Wt)

C	Si	Mn	P	S	Cr	Mo	Ni	V	Al	Cu	Sn
0.22	0.24	0.64	0.009	0.003	1.29	0.66	0.66	0.28	0.014	0.12	0.009

subsets. The training and test sub-sample sets were used to develop the neural network model; the validation subset was used to evaluate the performance of the resulting model. The result shows that a combination of ANN and FEM simulation performs well in estimation of C*. The framework of the methodology used is presented in Fig. 2.

EXPERIMENTS

The material used was a low alloy steel: 1% Cr 1% MoV (1CrMoV) rotor steel supplied by Buderus Edelstahlwerke. This material has a grain size between 14-34 mm and it was tested at 550°C. The material composition is shown in Table 1. The value of C* has been obtained from the load-point displacement rate following Eq. (6). Compact tension specimens were manufactured to the dimensions shown in Fig. 3. The experiments were carried out at constant load according to the recommendations of ASTM E1457-01. The

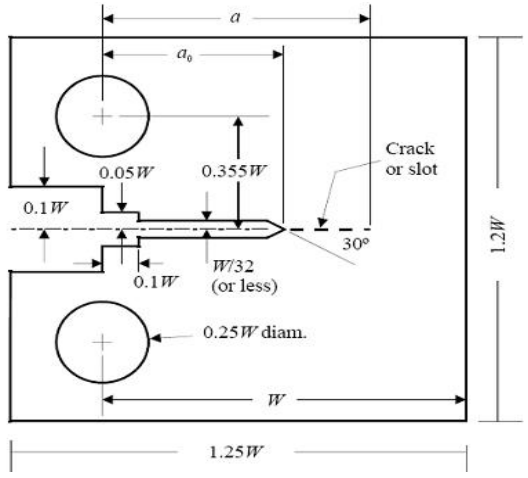

Fig. 3: Compact tension specimen used in the numerical analysis

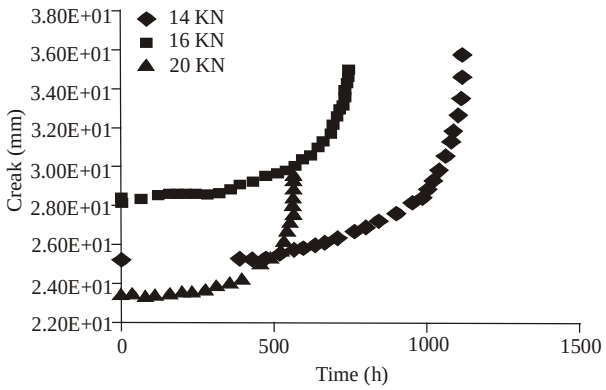

Fig. 4: Crack extension versus time for different loads at 550°C

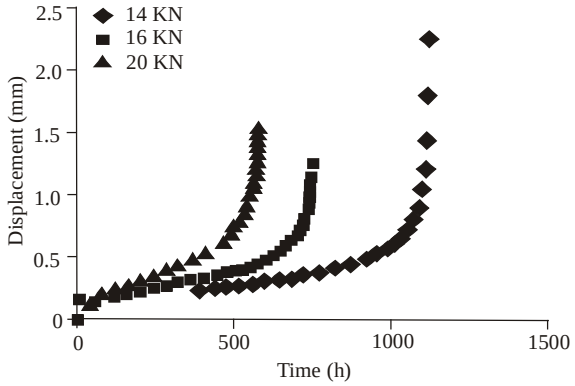

Fig. 5: Load line displacement versus time for different loads at 550°C

loading conditions were chosen to give failure times in the range of approximately 600 to 1200 h. All the specimens were provided with side grooves which were 10% deep on each side. The side grooves were not prepared until after a sharp fatigue crack had been introduced according ASTM standard E647-78T, at room temperature. In this way a flat straight fronted crack was produced prior to testing at elevated temperature. Extensometer was employed to monitor load point displacement in all the tests. A DC electrical potential method was used to measure crack growth in the specimens. With these techniques, it is estimated that crack extension could be recorded with an accuracy of ±0.1 mm using a linear calibration of voltage change taken between optical estimates of the initial a_0 and final crack lengths. It is believed that this procedure is more reliable than the formula given in ASTM E1457-01, for the test conditions used. The specimen was then heated to the required temperature. The loading was applied manually. The loading rate was kept to within one minute for the full load. The creep crack growth behavior of the 1CrMoV rotor steel at 550°C, obtained from tests on CT specimens and analyzed according to ASTM E1457-01, is shown in Fig. 4. As it can be seen little crack growth is experienced for the first approximately one-third of life. Also a crack extension of 0.5 mm is not observed until 80% of the life has been consumed. Examples of the load line deflection-time curves obtained for each test are presented in Fig. 5.

NUMERICAL DETAILS

The numerical evaluation was conducted on the same geometry and material as the experimental work. The specimen was of the compact tension geometry with specimen width, W = 50 mm and thickness, B_n = 6

Table 2: Creep properties (Norton uniaxial creep law)

Temperature (°C)	538	550	594
A	4.2E-27	1.3E-20	4E-21
n	10.2	6.5	7.06

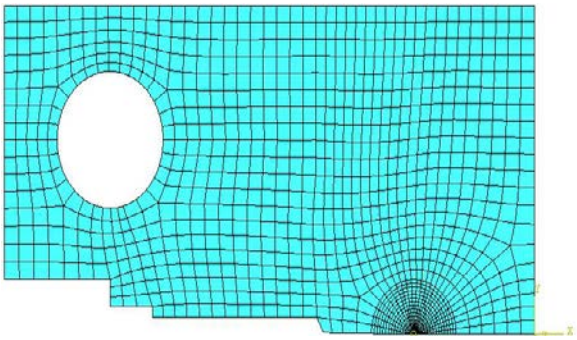

Fig. 6: 2D mesh used in the FEM of the compact geometry

mm. Calculations have been performed using elastic plus creep behavior and the creep response is described by Norton's secondary creep law. The creep properties of the material used are given in Table 2. The elastic module is 165 Gpa, the Poisson ratio, 0.3. The analysis was conducted on specimens with stationary crack length under constant applied forces. Fifty five cases were calculated using seven different crack lengths, three creep temperatures and three loading conditions. The finite element code used was ABAQUS/standard. Initially a comparison between 3D model and 2D model (plane stress and plane strain) was made. Both plane stress and plane strain analyses have been carried out. It was found the error to be less than 2-3 percent for plane stress condition; hence, for reducing computational time, a 2D model was used. A CPS8R element (8 nodes biquardratic, reduced integration plane stress elements) was used as shown in Fig. 6. A convergence study (mesh sensitivity) was performed to establish an optimum mesh size. The number of elements and nodes were more than 400 and 1300 respectively. These numbers varied slightly with crack length.

NEURAL NETWORKS

In the past decades, numerous studies have been reported on the development of the neural networks based on different architectures (Fausett, 1994; Karayiannis and Venetsanopoulos, 1993; Zurada, 1992). Basically, one can characterize neural networks by its important features, such as the architecture, the activation functions and the learning algorithm (Fausett, 1994). Three neural networks are employed for modeling the fracture mechanics parameter in this study.

- Hyperbolic Logistic sigmoid multi-layered learning perceptron with Resilient Back-Propagation algorithm (Resilient BP LOGMLP).

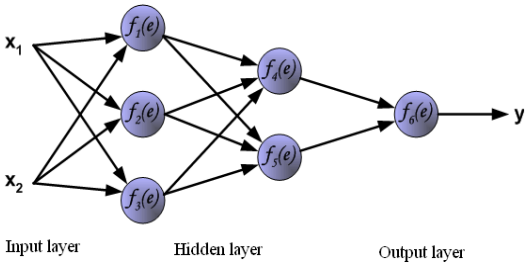

Fig. 7: Architecture of the multi-layered perceptron networks

- Hyperbolic Tangent sigmoid multi-layered learning perceptron with Resilient Back-Propagation algorithm (Resilient BP TANMLP).
- Hyperbolic Tangent sigmoid multi-layered learning perceptron with adaptive learning rate (Adaptive TANMLP).

Architectures: In Fig. 7 the architecture of the multi-layered perceptron networks is shown schematically. The number of hidden layers is critical for the convergence rate at the training stage of the network parameters. In addition, hybrid-learning algorithm for identifying the quasi-optimal membership function and other rule-based parameters has also been employed in this study. It is shown that network with one hidden layers would be sufficient in the multi-layered perceptron networks and the number of neurons was determined by an optimization method.

Activation function: For the neural networks shown in Fig. 7, the connections among the neurons are made by signal link designated by corresponding weighting. Each individual neuron represents an internal state, namely the activation, which is functionally dependent on the inputs. In general, the sigmoid functions(S-shaped curves), such as logistic functions and hyperbolic tangent functions, are adopted for representing the activation. In this study several different functions for activation have been employed for comparisons. The activation function for the LOGMLP model is a continuous logistic function given as:

$$f(t) = \frac{1}{1+e^{-\lambda t}} \tag{8}$$

where,
λ= A slope parameter

Similarly, the activation function for the TANMLP model is given as:

$$f(t) = \tanh(\frac{\lambda t}{2}) = \frac{1-e^{-\lambda t}}{1+e^{-\lambda t}} \tag{9}$$

where, λ = A slope parameter, same as in Eq. (8)

Algorithms: At the stage of training the neural networks, it is critical to see an appropriate algorithm, because the efficiency and convergence of the training are primary issue at this stage. That means the algorithm is for determining the weightings in order to accomplish the desired mapping between the inputs and the outputs. Based on a least-square approach, the quadratic error function E between the actual outputs and the networks outputs is expressed by:

$$E = \sum_p E_p = \sum_p \frac{1}{2}(T_p - Y_p)^2 \quad (10)$$

where,
T_p = Target value and
Y_p = Outputs of neural networks

In this study the delta learning rule (or namely the gradient descent) with momentum, the fast error back-propagation learning algorithm for updating its parameters, have been used. Considering the convergence criteria, both the least-squares method and the back propagation gradient descent method have been employed for the nonlinear parameters, respectively.

The performances of the networks were evaluated by the Root-mean-Square Error (RMS), which is defined as:

$$RMSE = \sqrt{\frac{1}{n}\sum_p (T_p - Y_p)^2} \quad (11)$$

where,
T_p = The actual tangent vector (i.e., experimental values)
Y_p = The predicted vector (training values).

As for the adaptive algorithm, the values of the learning coefficient have to be adequately increased when the RMSE of the current epoch is smaller than the RMSE of previous epoch. Otherwise, the values have to be adequately decreased when the RMSE of current epoch is larger than the RMSE of previous epoch.

RESULTS AND DISCUSSIONS

The value of C* has been obtained from the load-point displacement rate following Eq. (6). At the beginning of the loading elastic, plastic and creep deformation processes are likely to occur. With a constant applied force the elastic and plastic deformations are assumed to remain constant but the creep deformation is constantly changing with time. The load-line creep displacement rate $\dot{\Delta}^C$ is calculated using:

$$\dot{\Delta}^C = \dot{\Delta}^T - \dot{\Delta}^e - \dot{\Delta}^p \quad (12)$$

Table 3: Comparison of different training algorithms

Function	Technique	Time	Epochs	Average training error (%)	RMS
Traingdx	Variable learning rate	60	3600	4.200	2.7E-5
Trainrp	Resilient backpropagation	12	463	2.217	5.2E-7
Trainbfg	Bfgs quasi-newton	10	44	8.400	5.8E-4
Trainlm	Levenberg-Marquardt	1	6	12.750	9.6E-3

Table 4: Data for training, testing and validating the network

	a/w	P(N)	T(°C)	C*exp (MJ/m^2 h)	C*num (MJ/m^2 h)
1	0.544	16200	538		2.4 E-05
2	0.544	14100	538		2.12 E-06
3*	0.544	20000	538		1.12E-04
4	0.578	16200	538		6.98 E-05
5	0.578	14100	538		7.12 E-06
6	0.561	14100	538		3.49 E-06
7	0.561	16200	538		4.17 E-05
8	0.561	20000	538		1.97 E-04
9	0.53	14100	538		3.89 E-06
10*	0.53	16200	538		2.7 E-05
11	0.505	14100	538		3.54 E-06
12	0.505	16200	538		3.56 E-05
13	0.55	16200	538		3.42E-05
14	0.57	16200	538		5.61E-05
15	0.544	16200	550		4.71E-05
16	0.544	14100	550	2.49 E-06	
17	0.544	20000	550	1.66 E-04	
18	0.578	14100	550	3.63 E-05	
19	0.578	16200	550		1.51 E-04
20	0.578	20000	550	2.96 E-05	
21	0.561	16200	550	1.11 E-04	
22	0.561	14100	550	1.64 E-05	
23	0.561	20000	550	2.92 E-04	
24	0.53	14100	550	3.34 E-06	
25	0.53	16200	550		3.21 E-05
26	0.53	20000	550		1.14 E-04
27	0.505	14100	550	2.34 E-06	
28**	0.505	16200	550		2.75 E-05
29	0.505	20000	550	9.82 E-05	
30	0.55	14100	550		7.33E-06
31	0.57	14100	550		2.61E-05
32	0.55	16200	550		6.73E-05
33	0.57	16200	550		1.53E-04
34	0.57	20000	550		1.35E-04
35	0.544	16200	594		7.55E-05
36	0.544	14100	594		8.3 E-06
37	0.544	20000	594		2.65 E-04
38*	0.578	16200	594		1.73E-04
39	0.578	14100	594		2.6 E-05
40	0.578	20000	594		5.27 E-04
41**	0.561	14100	594		2.62 E-05
42	0.561	16200	594		1.36 E-04
43	0.561	20000	594		3.76 E-04
44	0.53	14100	594		5.88E-05
45	0.53	16200	594		5.3 E-05
46	0.53	20000	594		1.89 E-04
47	0.505	14100	594		5.11 E-06
48	0.505	16200	594		4.40 E-05
49	0.505	20000	594		1.62 E-04
50	0.55	14100	594		1.39E-05
51	0.57	14100	594		2.52E-05
52	0.55	20000	594		3.13E-04
53	0.57	20000	594		4.89E-04
54	0.55	16200	594		9.27E-05
55	0.57	16200	594		1.48E-04

*Used for testing the network; **Used for validating the network

where, $\dot{\Delta}^T$, $\dot{\Delta}^e$ and $\dot{\Delta}^p$ are the total, elastic and plastic displacement rates, respectively. Creep crack growth testing is normally carried out at loads where plastic deformation is insignificant and it is assumed that $\dot{\Delta}^C \succ \succ \dot{\Delta}^p$. Hence the creep strain rate can be calculated as (ASTM E1457-01, 2002):

$$\dot{\Delta}^C = \dot{\Delta}^T - \dot{\Delta}^e \quad (13)$$

Figure 8 shows the comparison of experimental with numerical C*at 550°C, good agreement between the line integral C* value and that obtained from Eq. (6) has been observed. The numerical analyses were performed under steady state creep and plane stress conditions and it is assumed that crack growth is in the plane of the crack. After confirming the validity of the model, number of computational calculations has been preformed to obtain C* at 538°C and 594°C. These results together with experimental results were used to train the ANN as shown in Table 3.

Based on experimental work, three inputs and one output in the networks was decided to be sufficient for this study as shown in Fig. 9. The ANN was designed and trained in MATLAB^{TM} environment. The calculations performed at each neuron are determined by an activation function, Eq. (8) and (9). The intensity of the signal passed between any two neurons depends on both the activation function and the weight of the connection. While connection weights will be modified during training of the network as observation patterns are passed along, activation functions are decided before the network training. The training process adjusts the weight of each neuron to an appropriate value. There are many available training algorithms such as Variable Learning Rate, Resilient back propagation, BFGS quasi-Newton and Levenberg-Marquardt. Comparison of different training algorithms technique is shown in Table 4. As it can be seen, the best approach which performed minimum errors is the Resilient back propagation algorithm (Freeman and Skapura, 1992; Fausett, 1994), hence, the Resilient range [-1, 1] before the training of the network

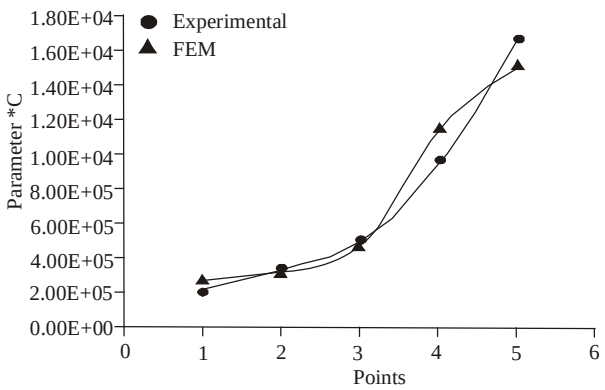

Fig. 8: Experimental and FEM Comparison at 550°C

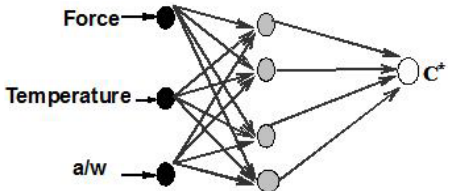

Fig. 9: A schematic of inputs and output

Table 5: Comparison of C* values based upon the Adaptive TANMLP model with the number of hidden nodes as the variable

Hidden layer nodes	6	7	8	9	10
Epochs	5000	5000	5000	5000	5000
RMS	3.848E-05	1.361E-05	3.050E-05	4.590E-05	7.923E-05
Average training error (%)	1.615	2.043	2.457	3.112	6.703
Average checking error (%)	5.174	2.459	3.158	7.662	5.634

Table 6: Comparison of C* values based upon the Resilient BP LOGMLP model with the number of hidden nodes as the variable

Hidden layer nodes	6	7	8	9	10
Epochs	972	1129	651	2012	798
RMS	1.864E-5	1.859E-5	1.861E-5	1.841E-5	1.825E-5
Average training error (%)	3.129	8.554	1.883	9.012	4.369
Average checking error (%)	5.235	1.185	3.843	4.657	6.032

Table 7: Comparison of C* values based upon the Resilient BP TANMLP model with the number of hidden nodes as the variable

First hidden layer nodes	6	7	8	9	10
Epochs	2836	440	227	761	359
RMS	9.358E-5	8.276E-6	3.957E-5	4.633E-7	2.341E-5
Average training error (%)	9.160	4.268	7.651	3.210	**2.584**
Average checking error (%)	3.780	5.947	4.143	1.215	6.954

(Malinov *et al*., 2001). The normalized values (X_n) for each data set (d_i) were calculated as:

$$X_n = \frac{2(d_i - d_{\min})}{d_{\max} - d_{\min}} - 1 \quad (14)$$

where, d_{max} and d_{min} are the maximum and minimum values of raw data, respectively. For determining the optimal architecture, networks with different number of neurons in the hidden layer have been designed and tested as shown in Table 5-7, in these three tables, the prediction, the training and the check errors, are defined as:

$$Error\% = \frac{(Experimental - \Pr ediction)}{Experimental} \quad (15)$$

The performance capability of each network has been examined based on percentage average training

Table 8: Final comparisons of the results

	Rp logmlp	Adapte tanmlp	Rp tanmlp
Hidden layer nodes	8	7	9
Epochs	651	5000	761
RMS	1.861E-5	1.361E-05	4.633E-7
Average training error (%)	1.883	2.043	3.210
Average checking error (%)	3.843	2.459	1.215

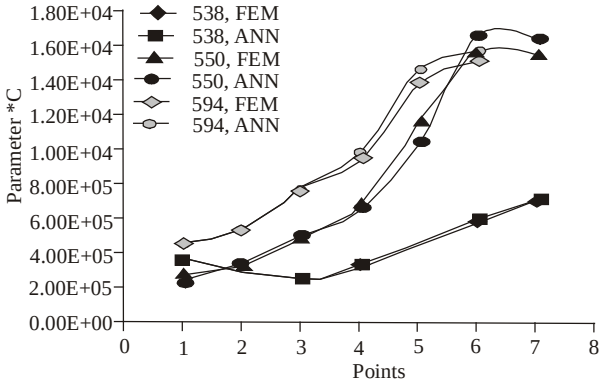

Fig. 10: Overall comparison of results at 538˚C, 550˚C, and 594˚C

error and percentage average checking error. The number of hidden neurons has been changed in order to optimize the structure of neural network. Also, the number of neurons in the hidden layer increases the amounts of connections and weights to be fitted. If this number (connections) is larger than the number of the data pairs available for training, although the neural network can still be trained, the case is mathematically undetermined (Sha and Edwards, 2007). The minimum learning inputs is Vemuri and Rogers (1994):

$$C = 1+\frac{N(I+T+1)}{T} \quad (16)$$

where,
C = The minimum learning inputs
N = Neurons in hidden layer
T = Output parameters
I = Input parameters

hence the number of neurons in hidden layer can be up to 10. By comparing the results, the number of neurons in the hidden layer was found to be 7 for the ADAPTIVE TANMLP model, 9 for the RP LOGMLP model and 8 for the RP TANMLP model. It is noted that the RP TANMLP model gives smaller check error than the others. Table 8 shows the final results for modeling the fracture mechanics parameter. From Table 8, it is identified that the RP TANMLP model with 9 neurons produced the best performance (3-9-1). The percentage average training error and percentage average checking error are 3.21 and 1.215% respectively. It would have been possible to optimize topology of the neural network, by utilized multi-objective genetic algorithms for training of the neural network. In this method the number of nodes in the hidden layer, the architecture of the network, the weights can be taken as variables and a Pareto front can be constructed by minimizing the training error along with the network size (Pettersson *et al*., 2007, 2009; Bhattacharya *et al*., 2009). The correlation between the predicted values of the optimum neural network model and the experimental data and finite element results for prediction of C* at 538°C, 550°C and 594°C are shown in Fig. 10. As it can be seen, the average error difference between experimental and ANN is 2%, while the number for experimental and FEM is 6%, which indicates the capability of ANN method.

CONCLUSION

In this study, creep crack growth behavior of low alloy steel was modeled by coupling experimental work, a non-linear fracture mechanics analysis based on a two dimensional finite elements and a neural network model. The neural network was used for prediction of C* at different temperatures. The finite element analysis data together with experimental data was used for training the various neural networks models. Based on the analysis of these results the following conclusions could be drawn:

- Creep crack growth tests are costly and time consuming. The numerical evaluation of (C*), involves a lot of parameters, a subtle change of any parameter will constitute a new scenario and a new simulation is needed to explore its behaviors. With the FEM simulation, it is difficult, time consuming and not pragmatic to conduct all the simulation. To address these issues, a new approach has been developed, which combines the FEM and ANN. This combination helps to reduce the simulation time and make it possible to search for the optimal parameters. All the validation results show the estimation of ANN can achieve satisfactory level.
- Three networks, namely the RP LOGMLP, ADAPTIVE TANMLP and the RP TANMLP have been trained and compared. It has been shown that the RP TANMLP model with one hidden layers of nine neurons produced the best performance (3-9-1).
- The average error difference between experimental and ANN is 2 %, while the number for experimental and FEM is 6%, which indicates the capability of ANN method.

REFERENCES

Bhattacharya, B., G.R.D. Kumar, A. Agarwal, S. Erkoç, A. Singh and N. Chakraborti, 2009. Analyzing Fe-Zn system using molecular dynamics: Evolutionary neural nets and multi-objective genetic lgorithms. Comput. Mater. Sci., 46(4): 821-827.

Di Lorenzo, R., G. Ingarao and F. Micari, 2006. On the use of artificial intelligence tools for fracture fore cast in cold forming operations. J. Mater. Process. Technol., 177: 315-318.

Djavanroodi, F. and K.M. Nikbin, 2006. The fracture mechanics concept of creep and creep/fatigue crack growth in life assessment. Int. J. Eng. Sci., 17: 1-7.

Freeman, J.A. and D.M. Skapura, 1992. Neural networks: Algorithms, Applications and Programming Techniques. Addison-Wesley, Reading. MA, pp: 401, ISBN: 13-9780201513769.

Fathi, A. and A.A. Aghakouchak, 2007. Prediction of fatigue crack growth rate in welded tubular joints using neural network. Int. J. Fatigue, 29: 261-275.

Fausett, L., 1994.Fundamentals of Neural Networks: Architectures, Algorithms and Applications. Prentice-Hall, Englewood Cliffs, N.J.

Hou, J.S., J.T. Guo, Y.X. Wub, L.Z. Zhou and H.Q. Ye, 2010. Effect of hafnium on creep behavior of a corrosion resistant nickel base superalloy. Mater. Sci. Eng. A., 527: 1548-1554.

Hwang, R., Y. Chen and H. Huang, 2010. Artificial intelligent analyzer for mechanical properties of rolled steel bar by using neural networks. Exp. Syst. Appl., 37: 3136-3139.

Karayiannis, N.B. and A.N. Venetsanopoulos, 1993. Artificial Neural Networks: Learning Algorithms, Performance Evaluation and Applications. Kluwer Academic, Amsterdam, the Netherlands.

Malinov, S., W. Sha and J.J. McKeown, 2001. Modelling the correlation between processing parameters and properties in titanium alloys using artificial neural network. Comput. Mater. Sci., 21: 375-394.

Mandal, S., V. Rakesh, P.V. Sivaprasad, S. Venugopal and K.V. Kasiviswanathan, 2009. Constitutive equations to predict high temperature flow stress in a Ti-modified austenitic stainless steel. Mater. Sci. Eng. A, 500: 114-121.

Mohanty, J.R., B.B. Verma, P.K. Ray and D.R.K. Parhi, 2010. Prediction of mode-I overload-induced fatigue crack growth rates using neuro-fuzzy approach. Exp. Syst. Appl., 37: 3075-3087.

Pettersson, F., N. Chakraborti and H. Saxen, 2007. A genetic algorithms based multi-objective neural net applied to noisy blast furnace data. Appl. Soft Comput., 7: 387-397.

Pettersson, F., A. Biswas, P.K. Sen, H. Saxen and N. Chakraborti, 2009. Analyzing leaching data for low-grade manganese ore using neural nets and multiobjective genetic algorithms. Mater. Manuf. Process., 24: 320-330.

Rice, J.R., 1968. Mathematical Analysis in the Mechanics of Fracture. In: Liebowitz, H. (Ed.), Treatise on Fracture. Academic Press, New York.

Sha, W. and K.L. Edwards, 2007. The use of artificial neural networks in materials science based research. Mater. Design, 28: 1747-1752.

Talebi Anaraki, M., M. Sanjari and A. Akbarzadeh, 2008. Modeling of high temperature rheological behavior of AZ61 Mg-alloy using inverse method and ANN. Mater. Design, 29: 1701-1706.

Tapkin, S., A. Cevik and U. Usar, 2009. Accumulated strain prediction of polypropylene modified marshall specimens in repeated creep test using artificial neural networks. Exp. Syst. Appl., 36: 11186-11197.

Toktas, I. and A.T. Ozdemir, 2011. Artificial neural networks solution to display residual hoop stress field encircling a split-sleeve cold expanded aircraft fastener hole. Exp. Syst. Appl., 38: 553-563.

Vemuri, V.R. and R.D. Rogers, 1994. Artificial Neural Networks-Forecasting Time Series. IEEE Computer Society Press, Los Alamitos, CA., USA, pp: 110, ISBN: 13- 9780818651205.

Webster, G.A. and R.A. Ainsworth, 1994. High Temperature Component Life Assessment. Chapman and Hall, New Jersey, pp: 344, ISBN: 13- 9780412585203.

Yatomi, M., N.P. O'Dowd, K.M. Nikbin and G.A. Webster, 2006. Theoretical and numerical modelling of creep crack growth in a carbon-manganese steel. Eng. Fracture Mech., 73: 1158-1175.

Zurada, J.M., 1992. Introduction to Artificial Neural Systems. West, USA, pp: 759, ISBN: 13-9780314933911.